ARTICLES

High-Resolution Microwave Spectroscopic and ab initio Studies of Propanoic Acid and Its Hydrates

Bin Ouyang and Brian J. Howard*

Physical and Theoretical Chemistry Laboratory, Department of Chemistry, University of Oxford, South Parks Road, Oxford OX1 3QZ, United Kingdom

Received: March 19, 2008; Revised Manuscript Received: June 20, 2008

High-resolution microwave spectra of the propanoic acid monomer (PPA) and two of its hydrates, the PPA−(H_2O) and the PPA−(H_2O)$_2$, were recorded using a pulsed nozzle Fourier transform microwave spectrometer. The rotational and centrifugal distortion constants of these species were determined. Agreements between the experimental and ab initio results of these constants, and of the planar moment of inertia, the dipole moments, and the orientation of the PPA relative to the H_2O confirm the geometry of the hydrates, i.e. H_2O binds to the carboxylic group of PPA and forms hydrogen-bonded ring complexes. The equilibrium constant and the change of entropy and enthalpy for the formation of PPA−(H_2O) were also derived, based on the calculation of partition functions, to evaluate the abundance of this monohydrate in the troposphere.

1. Introduction

Propanoic acid (PPA) is composed of an alkyl group (CH_3CH_2−), which is hydrophobic, and a carboxylic group (−COOH) which is hydrophilic. The coexistence of the two makes PPA behave more or less like a surfactant—it is both miscible with water and can also be removed from it by adding salt. As the third most abundant monocarboxylic acid in the atmosphere,[1] PPA can "capture" the H_2O molecules to form hydrates. It therefore acts as an effective component in the class of water soluble organic aerosols (WSOA)[2] that has been confirmed to be an important class of cloud condensation nuclei (CCN).[3] More importantly, the presence of the hydrophobic alkyl group can help the cloud droplets, especially those near the critical size formed on these nuclei, to overcome the barrier imposed by surface tension[4] and thus encourage the formation of clouds.

In previous microwave spectroscopic studies,[5–7] the structures of some acid−(H_2O) monohydrates were determined with the acids acting as hydrogen bond donor and the water as acceptor. In a few cases,[7–10] the acid−(H_2O)$_2$ dihydrates and acid−(H_2O)$_3$ trihydrate have also been successfully observed. The structures of these hydrates can be deduced from the rotational constants through fitting of the spectra. This deepens our understanding of the hydrogen-bonding interactions between the different acid molecules and the ubiquitous H_2O molecules.

Formation of hydrates vividly mirrors the condensation of H_2O molecules on the PPA, one of the WSOA, on a molecular scale. Inspired by this, we studied the hydration of PPA in the gas phase using Fourier transform microwave spectroscopy. The high-resolution rotational spectra of the acid and its mono- and dihydrates were recorded and fitted. It is shown that −COOH is the active site to which the H_2O molecules bind. Both hydrates possess hydrogen-bonded ring structures. High-level ab initio calculations were performed to assist structural assignment and to give the binding energy of the hydrates. The partition function of the PPA−(H_2O) dimer has also been calculated, and the equilibrium constant, the change of enthalpy, and entropy at different temperatures for this very first hydration step were derived.

2. Experimental Details

All experiments were performed on a pulsed nozzle Fourier transform microwave spectrometer (FTMS). Details of the free-jet Fourier transform microwave spectrometer have been presented before.[10] An outline of the spectrometer is briefly summarized below.

Microwave pulses of 2 μs are introduced by an antenna into a Fabry−Perot cavity to excite the molecules. The cavity is composed of two confocal aluminum mirrors with diameter of 65 cm and radius of curvature of 60 cm. The distance between the two mirrors is about 50 cm and can be tuned to support microwave frequencies in the range of 3−18 GHz. The cavity is continuously evacuated by a diffusion pump to keep the pressure below 10^{-4} torr.

The gas sample was prepared by bubbling helium through a mixed solution of PPA and H_2O (50:1, v/v). The molar ratio of PPA to H_2O in the gas phase was approximately 2:1. The gas flow was pulsed through a solenoid valve into the high-vacuum cavity and then underwent supersonic expansion during which the molecules were cooled and the complexes were formed. The complexes were then excited by the microwave pulses. After the cavity ring-down of the input microwave pulse, the emission of the excited molecules was recorded by the same antenna used for excitation, mixed in two stages down to a frequency centered at 2.5 MHz, digitized by a 10 MHz analogue-to-digital card, and then transferred to a computer for further analysis. Due to the coaxial setup of the gas nozzle and the antenna, all emission signals were split into Doppler doublets. The arithmetic mean of the doublets was taken as the true transition frequency.

* Author to whom correspondence should be addressed. Fax: +44 1865 275410. E-mail: brian.howard@chem.ox.ac.uk.

10.1021/jp802422b CCC: $40.75
Published on Web 08/16/2008

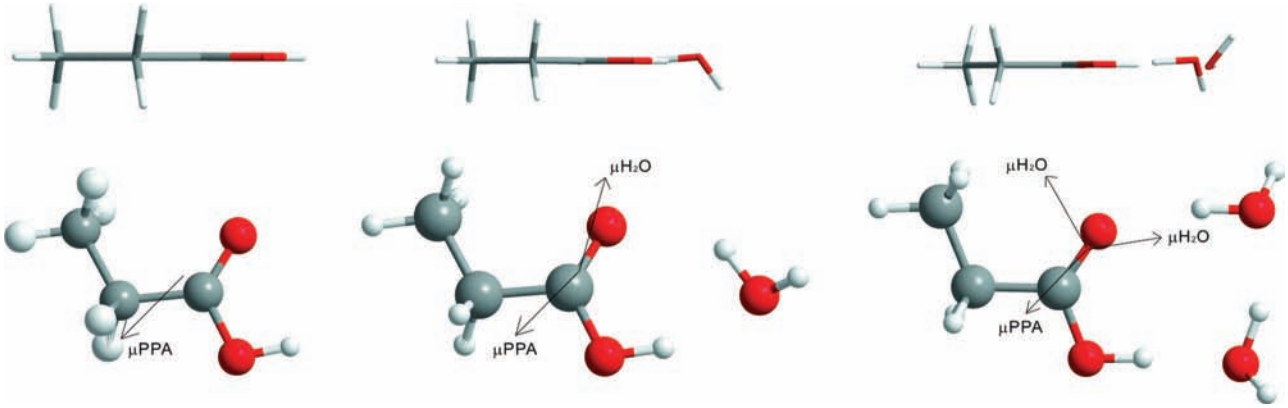

Figure 1. Global minimum conformation of the PPA monomer, the PPA−(H_2O), and the PPA−(H_2O)$_2$ hydrates. The equatorial pictures of them are displayed directly above them.

TABLE 1: Ab initio Rotational Constants of PPA, PPA−(H_2O), and PPA−(H_2O)$_2$[a]

parameter	PPA	PPA−(H_2O)	PPA−(H_2O)$_2$
A/MHz	10 169.06	8163.20	3628.06
B/MHz	3860.86	1627.87	1103.34
C/MHz	2896.94	1383.52	857.56
P_c[b]/u Å^2	3.07	3.54	4.01
μ_a[c]/Debye	0.15	0.34	0.27
μ_b/Debye	1.49	0.13	0.11
μ_c/Debye	0.00	1.18	0.03

[a] The calculations were performed at the MP2/6-311++G(2df, 2pd) level with counterpoise corrections made in the geometry optimizations. [b] Planar moment of inertia P_c. The conversion factor between moment of inertia *I* and rotational constants is taken as 505 379 MHz u Å^2. [c] Dipole moments based on the MP2 densities.

Scan from 3 to 18 GHz was carried out at steps of 0.5 MHz in an automated manner. Averaging of 1000−10 000 shots was performed to achieve reasonable signal to noise ratios (S/N).

3. Results and Discussion

3.1. Assignments of Microwave Spectra. First, the known transitions of the H_2O dimer[11] were removed from the list of observed lines. With the rotational constants reported by Stiefvater,[12] the transitions of the PPA monomer were also readily located. Searches for the PPA hydrates were then performed within the unassigned lines, which were generally weak.

To assign the microwave spectra of the hydrates, their geometries were first optimized by ab initio calculations and the rotational constants and dipole moments of them were obtained to predict the position and relative intensity of the rotational transitions. The Møller−Plesset second-order perturbation method (MP2)[13] coupled with the 6-311++G(2df,2pd) basis set was used throughout the geometric optimizations. Counterpoise corrections were made to remove the basis set superposition error (BSSE).[14] Core electrons were frozen in the calculations. All calculations were performed using the Gaussian'03 package.[15] The global minimum conformations of the PPA monomer and two of its hydrates are shown in Figure 1. Their rotational constants and dipole moments are listed in Table 1. The Cartesian coordinates of all the atoms in the principal axis system are given in Supporting Information part A. Interested readers can obtain more detailed information, e.g. the calculated bond length and bond angles, from it.

Using the theoretical rotational constants, the rotational spectra with $J \leq 8$ in the 3−18 GHz region were predicted for both hydrates. Of the predicted lines, the three *a*-type *R*-branch transitions, $J_{0,J} \leftarrow (J-1)_{0,J-1}$, $(J+1)_{0,J+1} \leftarrow J_{0,J}$ and $J_{1,J} \leftarrow (J-1)_{1,J-1}$, were first looked for. As both hydrates are near-prolate top molecules, the simultaneous fitting of these three transitions allows the values of $(B+C)$ and $(B-C)$ to be pinned down. The value of rotational constant *A*, however, can not be determined to a similar accuracy because the transition frequencies of these three lines are not sensitive to it. As a result, *A* was fixed at its ab initio value while *B* and *C* were allowed to float. After a number of trials, reasonable fits were achieved. With the preliminarily fitted rotational constants, *a*-type transitions involving the other *J*'s were easily located. Some of the $K_a = 2$ doublets of the *a*-type, *R*-branch transitions were also observed, though with a much reduced intensity. A full list of the observed transitions can be found in Tables 2−4. The inclusion of several $K_a = 0$ and $K_a = 2$ transitions permitted the magnitude of the *A* rotational constant to be determined within an error of about ±1 MHz. The SPFIT and SPCAT programs of Pickett[16] were used in the above spectral predictions and fits.

When the quartic centrifugal distortion constants in the Watson-S representation were included in the fitting, the root-mean-square of the error for these *a*-type transitions was reduced from about 40 kHz to less than 3 kHz for both hydrates. The latter value is fairly similar to the experimental uncertainty (2 kHz), which suggests that the standard Hamiltonian developed

TABLE 2: Observed Transitions of the *A*-State of PPA Monomer

transition	ν_{obs}/MHz	$\Delta\nu$[a]/MHz
	a-type	
$1_{0,1} \leftarrow 0_{0,0}$	6693.0549	−0.0012
$2_{1,2} \leftarrow 1_{1,1}$	12 443.3766	0.0044
$2_{0,2} \leftarrow 1_{0,1}$	13 288.5526	−0.0008
$2_{1,1} \leftarrow 1_{1,0}$	14 328.7840	−0.0051
	b-type	
$1_{1,1} \leftarrow 0_{0,0}$	13 030.5368	−0.0015
$1_{1,0} \leftarrow 1_{0,1}$	7280.1971	0.0020
$2_{0,2} \leftarrow 1_{1,1}$	6951.0732	0.0020
$2_{1,1} \leftarrow 2_{0,2}$	8320.4326	0.0018
$3_{0,3} \leftarrow 2_{1,2}$	14 203.3834	0.0014
$3_{1,2} \leftarrow 3_{0,3}$	10 053.4284	0.0014
$4_{1,3} \leftarrow 3_{2,2}$	10 779.4258	−0.0006
$4_{1,3} \leftarrow 4_{0,4}$	12 641.8874	−0.0005
$4_{2,2} \leftarrow 4_{1,3}$	17 315.4512	−0.0009
$5_{1,4} \leftarrow 5_{0,5}$	16 201.2147	0.0002
$5_{2,3} \leftarrow 5_{1,4}$	16 934.1264	0.0001
$6_{2,4} \leftarrow 6_{1,5}$	17 269.3633	0.0002

[a] $\Delta\nu = \nu_{obs} - \nu_{calc}$.

TABLE 3: Observed Transitions of PPA−(H_2O)

transition	ν_{obs}/MHz	$\Delta\nu^a$/MHz
	a-type	
$2_{1,2} \leftarrow 1_{1,1}$	5750.2782	0.0008
$2_{0,2} \leftarrow 1_{0,1}$	5985.3598	−0.0008
$3_{0,3} \leftarrow 2_{0,2}$	8961.6368	0.0011
$3_{1,3} \leftarrow 2_{1,2}$	8621.3458	−0.0011
$3_{1,2} \leftarrow 2_{1,1}$	9346.1819	−0.0010
$4_{0,4} \leftarrow 3_{0,3}$	11 918.4124	−0.0010
$4_{1,4} \leftarrow 3_{1,3}$	11 487.6886	0.0001
$4_{1,3} \leftarrow 3_{1,2}$	12 453.5999	0.0005
$4_{2,3} \leftarrow 3_{2,2}$	11 978.7051	0.0088
$4_{2,2} \leftarrow 3_{2,1}$	12 044.0458	−0.0050
$5_{0,5} \leftarrow 4_{0,4}$	14 849.7877	−0.0022
$5_{1,5} \leftarrow 4_{1,4}$	14 347.9807	0.0010
$5_{1,4} \leftarrow 4_{1,3}$	15 553.8405	0.0014
$5_{2,4} \leftarrow 4_{2,3}$	14 965.0887	−0.0052
$5_{2,3} \leftarrow 4_{2,2}$	15 094.9283	0.0017
$6_{1,6} \leftarrow 5_{1,5}$	17 201.1065	0.0004
$6_{0,6} \leftarrow 5_{0,5}$	17 750.8803	0.0007

[a] $\Delta\nu = \nu_{obs} - \nu_{calc}$.

TABLE 4: Observed Transitions of PPA−(H_2O)$_2$

transition	ν_{obs}/MHz	$\Delta\nu^a$/MHz
	a-type	
$4_{0,4} \leftarrow 3_{0,3}$	7674.032	−0.0017
$4_{1,4} \leftarrow 3_{1,3}$	7316.8817	0.0014
$4_{1,3} \leftarrow 3_{1,2}$	8293.9763	0.0011
$5_{0,5} \leftarrow 4_{0,4}$	9481.1582	0.0003
$5_{1,5} \leftarrow 4_{1,4}$	9118.8725	−0.0036
$5_{1,4} \leftarrow 4_{1,3}$	10 330.3641	−0.0008
$5_{2,4} \leftarrow 4_{2,3}$	9761.6168	0.0013
$5_{2,3} \leftarrow 4_{2,2}$	10 079.7013	0.0012
$6_{0,6} \leftarrow 5_{0,5}$	11 236.678	0.0016
$6_{1,6} \leftarrow 5_{1,5}$	10 906.2718	0.0008
$6_{1,5} \leftarrow 5_{1,4}$	12 337.9425	0.0011
$6_{2,5} \leftarrow 5_{2,4}$	11 682.9233	−0.0023
$6_{2,4} \leftarrow 5_{2,3}$	12 204.5953	−0.0020
$7_{0,7} \leftarrow 6_{0,6}$	12 953.8586	0.0011
$7_{1,7} \leftarrow 6_{1,6}$	12 679.1737	0.0006
$7_{2,6} \leftarrow 6_{2,5}$	13 587.7821	0.0010
$7_{2,5} \leftarrow 6_{2,4}$	14 349.886	0.0009
$7_{1,6} \leftarrow 6_{1,5}$	14 307.3161	−0.0011
$8_{1,8} \leftarrow 7_{1,7}$	14 438.6755	0.0000
$8_{0,8} \leftarrow 7_{0,7}$	14 650.0153	−0.0013
	b-type	
$4_{1,4} \leftarrow 3_{0,3}$	9302.7941	−0.0007
$5_{1,5} \leftarrow 4_{0,4}$	10 747.6379	0.0007

[a] $\Delta\nu = \nu_{obs} - \nu_{calc}$.

for nonrigid asymmetric molecules is sufficient to fit the rotational spectra of the two hydrates.

Searches for *b*- and *c*-type transitions of both hydrates were carefully performed within ±10 MHz of their predicted frequencies. However, only two of the *b*-type transitions of PPA−(H_2O)$_2$ were recorded. The lack of *b*- and *c*-type transitions prohibits us from determining the *A* rotational constants to similar accuracies as *B* and *C*. Moreover, the values of the D_K centrifugal distortion constants of both hydrates cannot be determined as no *b*- or *c*-type transitions with $K_a \geq 2$ were recorded. A full list of the experimental rotational and centrifugal distortion constants are given in Table 5.

Small splittings of tens of kHz were observed in the *b*-type transitions of the PPA monomer. An illustration of this splitting was given in Figure 2. Given that the PPA monomer is a closed-shell molecule which contains no nucleus with spin larger than 1, no magnetic, quadrupole or spin-rotation hyperfine splittings

TABLE 5: Experimental Rotational Constants and Centrifugal Distortion Constants

parameter	PPA	PPA−(H_2O)	PPA−(H_2O)$_2$
A/MHz	10,155.3785 (33)[a]	8,167.312 (305)	3,627.7231 (71)
B/MHz	3,817.88663 (116)	1,618.81207 (149)	1,102.64688 (99)
C/MHz	2,875.17221 (117)	1,377.15747 (115)	857.26038 (65)
P_c[b]/u Å^2	3.1813	3.5485	4.0566
D_J/kHz	0.685 (52)	0.4115 (136)	0.1450 (45)
D_K/kHz	2.89 (154)	N/A	N/A
D_{JK}/kHz	3.78 (41)	−0.903 (190)	0.692 (92)
d_1/kHz	−0.1866 (136)	−0.0757 (137)	−0.0415 (43)
d_2/kHz	−0.0076 (112)	−0.0071 (91)	−0.00841 (240)
N[c]	16	17	23
σ_{rms}[d]/kHz	2.03	2.93	1.41

[a] Values in parentheses are one standard deviation of the fitted value in units of the last digit quoted. [b] Planar moment of inertia, as calculated from $P_c = (I_a + I_b - I_c)/2 = \Sigma_i m_i c_i^2$. The conversion factor between moment of inertia *I* and rotational constants is taken as 505 379 MHz u Å^2. [c] Number of lines included in fitting. [d] Root-mean-square of the errors.

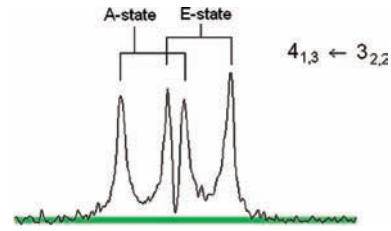

Figure 2. Internal rotation splitting in the transition $4_{1,3} \leftarrow 3_{2,2}$ of the PPA monomer with the *A* and *E* states labeled. The splittings within the same state are the typical Doppler splittings.

should occur. Also the spin−spin interactions of the protons are likely to be small. Hence, we attempted to attribute this to the internal rotation of the methyl group in the molecule. Fitting of these splittings with the Hamiltonian considering internal rotation yielded satisfactory results. Two states of different symmetries, the *A* and the *E* as defined by the C_3 operation,[17] were present in the spectrum as shown in Figure 2. The program of Hartwig and Dreizler[18] was used in the fitting. The observed and the fitted *A*−*E* splittings are listed in Table 6. The orientation of the rotation axis and the barrier to internal rotation of the methyl group obtained from the fitting are also given in the same table. It is noteworthy that splittings due to internal rotation have been previously observed by Stiefvater for PPA.[12] Restricted by the resolution of the spectrometer, he made use of transitions with much larger *A*−*E* splittings, mostly on the scale of several tens of MHz, to determine the internal rotation parameters. His fitted parameters are in reasonable agreement with the current study. For a better comparison, we have also fitted the transitions using the Watson-A representation, and the results are given in Supporting Information part B.

3.2. Structure and Tunneling Motion of PPA−(H_2O). The agreement between the ab initio and experimental rotational constants (Table 1 and Table 5) provides the first piece of evidence for the structure of the hydrate, i.e. H_2O binds to the carboxylic group to form the hydrogen-bonded hydrate.

A second piece of evidence to confirm the structure is supplied by the experimental dipole moments. Although not explicitly determined, the magnitude of the *a*- and *b*-dipole moments could be roughly estimated from the dependence of the intensity of the corresponding transitions upon the microwave power. For PPA−(H_2O), the *a*-dipole moment was found to be about 0.1−0.2 Debye, while the *b*-dipole moment was reckoned to be similar or even smaller. The small dipole moment

TABLE 6: $A-E$ Splittings of PPA Monomer and the Internal Rotation Parameters Derived from the Fitting of Them

transition	$(\nu_A-\nu_E)_{obs}$/kHz	$(\nu_A-\nu_E)_{calc}$/kHz
a-type		
$1_{1,1} \leftarrow 0_{0,0}$	37.4	38.9
$1_{1,0} \leftarrow 1_{0,1}$	41.3	38.5
$2_{0,2} \leftarrow 1_{1,1}$	−34.2	−31.4
$2_{1,1} \leftarrow 2_{0,2}$	43.1	41.1
$3_{0,3} \leftarrow 2_{1,2}$	−26.5	−26.3
$3_{1,2} \leftarrow 3_{0,3}$	46.7	44.9
$4_{1,3} \leftarrow 3_{2,2}$	−91.5	−90.9
$4_{1,3} \leftarrow 4_{0,4}$	50.9	50.1
$4_{2,2} \leftarrow 4_{1,3}$	98.9	98.8
$5_{1,4} \leftarrow 5_{0,5}$	59.2	57.5
$5_{2,3} \leftarrow 5_{1,4}$	91.3	93.2
$6_{2,4} \leftarrow 6_{1,5}$	84.5	87.6
internal rotation parameters		
V_3/cm^{-1} [a]	810.7 ± 3.7	
δ/deg[b]	34.0	
ϵ/deg	0.0	

[a] The 3-fold barrier to internal rotation. The moment of inertia of the methyl group, I_α, was taken as 3.136 u Å.[12] [b] The orientation angle δ is the angle between the internal rotation axis and the principal *a*-axis, and ϵ is the angle between the principal *b*-axis and the projection of the internal rotation axis onto the *bc* plane. Given that the $A-E$ splittings shown in the table are not sensitive to ϵ, we have fixed it to 0 in line with the fact that the PPA monomer has a plane of symmetry with respect to the *bc* plane.

of the hydrate reflects the fact that the dipole moment vectors of the PPA and H_2O are opposing rather than enhancing each other. This is effectively satisfied when H_2O binds to the carboxylic group of PPA. Indeed, with the geometries shown in Figure 1, the dipole moment of PPA−(H_2O) based on the MP2 density is quite close to its experimental value, which again validates the structure.

Furthermore, the binding energy of PPA−(H_2O), with H_2O binding to the carboxylic group, is at least 1000 cm^{-1} larger than those of all other conformations. This suggests that the structure of PPA−(H_2O) shown in Figure 1 is the global minimum conformation and is thus the predominant species formed in the supersonic expansion.

The PPA monomer has a plane of symmetry with only four hydrogen atoms in the alkyl-group standing out of the symmetry plane.[12] Its planar moment of inertia, denoted as P_c, is about double that of the methyl group in acetic acid.[19] From P_c, the average of the vertical distances of the four out-of-plane alkyl-hydrogen atoms to the plane was calculated to be 0.892 Å.

An increased value of P_c for PPA−(H_2O) compared to the PPA monomer (Table 5) suggests that other atoms besides the alkyl-hydrogen atoms are lying out of the plane. This compares well with the ab initio predictions, i.e. the unbound hydrogen in H_2O is protruding out of the plane and contributes significantly to P_c. The *c*-dipole moment of this complex at its equilibrium structure is predicted by ab initio calculations to be 1.3 Debye. However, despite this apparently large dipole moment, all *c*-type transitions are missing due to the large amplitude tunneling motions. A full-length discussion on the possible tunneling motions of the unbound hydrogen can be found in reference.[10] Of these motions, the inversion of the unbound hydrogen has the lowest barrier and the smallest reduced mass and is therefore the easiest to achieve. A semiclassical calculation[10] showed that the tunneling frequency associated with this motion is about 14 cm^{-1} and is at least 1 or 2 orders of magnitude larger than the others.

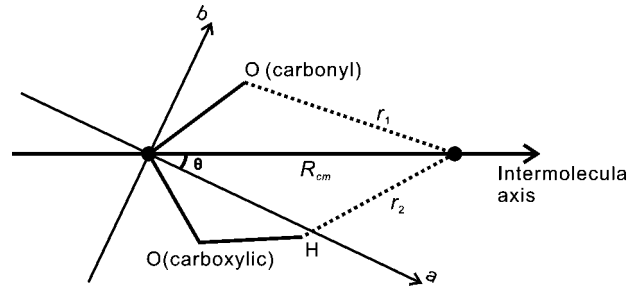

Figure 3. Orientation of the principal *a*- and *b*-axes of the PPA monomer relative to the intermolecular axis.

TABLE 7: Comparison between Experiment and ab initio (MP2/6-311++G(2df,2pd)) Predictions of Structural Parameters

	experiment	ab initio
θ/deg	24.8	24.9
R_{cm}/Å	3.619	3.621
r_1/Å	2.775	2.781
r_2/Å	1.868	1.867

A full structural analysis requires significant isotopic substitution. However, there is still information on the structure that we can extract. To analyze this, we made use of the fact that except for a very light atom, i.e. the unbound hydrogen atom in the H_2O molecule, the other part of PPA−(H_2O) still possesses a near plane of symmetry. As a result, the *ab* plane of the PPA monomer and that of the hydrate can be considered as overlapping, and the intermolecular axis connecting the center-of-mass of the two monomers can be considered as lying in the plane within a good approximation. This is shown in Figure 3. The angle θ between the *a* principal axis of the PPA monomer and the intermolecular axis determines the magnitude of the moments of inertia of PPA−(H_2O) around the *a* and *b* principal axes of this complex. Therefore, we can determine θ and R_{cm} using the following equations:

$$\sin^2\theta = \frac{I_A(\mu R_{cm}^2 + I_a + I_b - I_A) - I_a(\mu R_{cm}^2 + I_b)}{(\mu R_{cm}^2)(I_b - I_a)} \quad (1)$$

$$\text{with } \mu R_{cm}^2 = \frac{I_C - I_c}{2} \quad (2)$$

Derivation of eq 1 is given in Supporting Information part C. I_a, I_b, and I_c in eqs 1 and 2 are the moments of inertia of the PPA monomer around each principal axis, and I_A, I_B, and I_C are those of the complex. The term μ is the reduced mass of PPA and H_2O, and R_{cm} is the distance between centers of mass of the two. All of these are known from the measured rotational constants of the corresponding species.

In deriving the above equations, however, three assumptions were needed (for details see Supporting Information part C). Some minor corrections to the moments of inertia of both the monomers and the complex were therefore necessary to examine the propagated changes of θ. After considering these corrections, we found that θ dropped by about 1.7°. We need to note that the value of θ shown in Table 7 is the corrected result.

By substituting the experimentally determined moments of inertia into eqs 1 and 2, the value of θ and R_{cm} were calculated. With the information on θ and R_{cm} and also on the known structure of the PPA monomer,[12] it is possible to calculate the distances between the carbonyl oxygen and the carboxylic hydrogen atoms of the PPA monomer to the center of mass of H_2O. They are denoted as r_1 and r_2 in Figure 3. The values of

TABLE 8: Binding Energies, Calculated As the Modulus of the Energy of the Complex Relative to the Sum of the Separate Monomers, at the MP2 Level with Different Basis Sets

	D_e			
	PPA−$(H_2O)^a$		PPA−$(H_2O)_2{}^b$	
	HF	E2	HF	E2
aug-cc-pVDZ	2226.3	869.0	5022.2	1506.3
aug-cc-pVTZ	2222.0	1146.4	5098.3	1940.9
aug-cc-pVQZ	2231.3	1252.3	−	−
↓				
aug-cc-pV∞Z	2231.3	1342.3[c] 1346.0[d]	5098.3	2236.7[c]
	D_e/n^e			
aug-cc-pV ∞ Z	1787.7	2445.0		

[a] With geometry optimized at the MP2/aug-cc-pVTZ level. [b] With geometry optimized at the MP2/6-311++G(2df,2pd) level. [c] Extrapolated with the expression $E_X = E_\infty + A \times \exp(-1.21843X + 0.06291X^2)$ (ref 25) for the TZ-QZ basis sets of PPA−(H_2O) and for the DZ-TZ basis sets of PPA−$(H_2O)_2$, in which X equals to 2, 3, and 4 for the DZ, TZ, and QZ basis sets, respectively. The coefficients −1.21843 and 0.06291 were the optimized values from the regression of the E2 energies, all calculated using MP2/aug-cc-pVXZ, of 7 model molecules selected by Klopper.[27] [d] Extrapolated with the expression $E_X = E_\infty + A(X+1)^{-4} + B(X+1)^{-5}$ (ref 26) for the DZ-TZ-QZ basis sets. [e] The number of hydrogen bonds formed.

θ, R_{cm}, r_1, and r_2 are listed in Table 7. Both the experimental and the theoretical values are given for comparison. They are generally in good agreement.

The lengths of the hydrogen bonds were dependent not only on the values of r_1 and r_2 but also on the orientation of the H_2O molecule. As the latter was not derivable from the above calculations, we were unable to determine the hydrogen bond lengths to a high level of accuracy. An approximate calculation using the orientation angle of H_2O given by ab initio calculations suggested that the length of the hydrogen bond C═O···HOH was 1.980 ± 0.080 Å while that of COOH···OH_2 was 1.838 ∓ 0.006 Å. The associated errors correspond to a ±5° in-plane tilt of the hydrogen-bonded O−H bond of H_2O. Note the signs, as the errors are correlated.

3.3. Enhanced Hydrogen Bonding in PPA−$(H_2O)_2$. Similar agreement for the rotational constants, the dipole moments, and the planar moment of inertia found in the cases of the PPA−$(H_2O)_2$ (Tables 1 and 5) firmly supports the structure of this hydrate as shown in Figure 1. Two H_2O molecules forming a somewhat distorted H_2O dimer[20] are complexed with PPA to form a ring structure with three hydrogen bonds.

Significant enhancement of the hydrogen-bonding strength is demonstrated by ab initio calculations in two aspects. First, the lengths of the hydrogen bonds were predicted to be considerably shorter in PPA−$(H_2O)_2$ than in PPA−(H_2O). The length of the hydrogen bond C═O···HOH is reduced by 0.16 Å while that of COOH···OH_2 is reduced by 0.12 Å at the level of MP2/6-311++G(2df,2pd). Second, the binding energies, D_e, of both hydrates were calculated using the MP2 method with the different aug-cc-pVXZ (X = D, T, and Q) basis sets developed by Dunning et al.[22,23] With the standard methods,[25,26] D_e was then extrapolated to its complete basis set (CBS) limit. As shown in Table 8, the binding energy per hydrogen bond, i.e. D_e divided by the number of hydrogen bonds formed, is 30% higher for the PPA−$(H_2O)_2$ than that for the PPA−(H_2O), again indicating a stronger hydrogen-bonding effect in the former hydrate.

3.4. Equilibrium Constant and Thermodynamics of PPA−(H_2O). With the standard equations of statistical mechanics,[21] it is possible to calculate the equilibrium constant of the PPA−(H_2O) as

$$K_{p,PPA-(H_2O)} = (q^{\ominus}_{PPA-(H_2O)} e^{\frac{D_0}{kT}} N_A 2)/(q^{\ominus}_{PPA} q^{\ominus}_{(H_2O)}) \qquad (3)$$

in which $q^{\ominus}_{PPA-(H_2O)}$, $q^{\ominus}_{PPA}$, and $q^{\ominus}_{H_2O}$ are the overall (translational, rotational, and vibrational) partition functions of the three species at a molar volume at 1 bar, D_0 is the dissociation energy of PPA−(H_2O) obtained by subtracting the zero point energy (ZPE) correction from the binding energy, k_B is the Boltzmann constant, T is the temperature, and N_A is the Avogadro constant. The extra "2" in the numerator comes from the fact that the PPA−(H_2O) has two equivalent geometries, with the unbound hydrogen atom in H_2O standing up and down the mirror plane (Figure 1), and both contribute equally to the partition functions of the complex.

TABLE 9: Harmonic Vibrational Frequencies (in inverse centimeters) of the PPA and the H_2O Monomers and of the PPA−(H_2O) Monohydrate at the Level of MP2/aug-cc-pVDZ[a]

	PPA or H_2O		PPA−(H_2O)
	ab initio	experiment	ab initio
	intermolecular modes		
χ_1			70
χ_2			131
χ_3			175
χ_4			249
χ_5			345
χ_6			599
	intramolecular modes[b]		
ν_1[c]	50		−5
ν_2	220		2
ν_3	249		29
ν_4	464	465.4	20
ν_5	524	510.7	36
ν_6	604	607.7	28
ν_7	649	625.5	213
ν_8	802	804.5	1
ν_9	822	813.8	20
ν_{10}	1017		2
ν_{11}	1092	1066.4	1
ν_{12}	1102		14
ν_{13}	1159	1138.5	60
ν_{14}	1277		0
ν_{15}	1295		69
ν_{16}	1395	1377.7	7
ν_{17}	1412	1385.2	26
ν_{18}	1452	1426.3	2
ν_{19}	1486	1457.7	0
ν_{20}	1492	1466.0	1
ν_{21}	1786	1776.1	−29
ν_{22}	3081	2937.9	−1
ν_{23}	3083	2954.2	0
ν_{24}	3132		0
ν_{25}	3175	2995.8	−1
ν_{26}	3179	3002.5	−1
ν_{27}	3738	3569.2	−271
ν_1'[d]	1622	1595.0	−2
ν_2'	3803	3651.7	−140
ν_3'	3938	3755.8	−48

[a] Available experimental values are also listed for comparison. [b] Intramolecular vibrational frequencies of the complex in column 4 are written as $\nu_{complex} - \nu_{monomer}$. [c] Vibrations within the PPA fragment. Experimental values were the average of those of Maçôas[30] and Sander.[31] [d] Vibrations within the H_2O fragment.

The translational and rotational parts of the partition functions are easy to calculate since the masses and the rotational constants of the relevant species are known to a high accuracy. However, calculation of the vibrational partition functions and the dissociation energy of the hydrate requires a reasonable knowledge of the vibrational frequencies, ν, and the binding energy, D_e. Due to the lack of experimental data, both ν and D_e were obtained from ab initio calculations.

The binding energy of PPA$-H_2O$ was calculated at the MP2/CBS level (see section 3.3) to remove the error caused by the incompleteness of the basis set. It is not possible to use a higher-order correlation method, as restricted by the size of the system, to examine the sensitivity of D_e to higher-order terms of the correlation energy. For many hydrogen-bonded systems, D_e obtained at the MP2 level are found to be very similar to those at the CCSD(T) level,[26,28,29] suggesting that either the higher-order correlation terms contribute little to D_e or that there is a cancelation of errors in the MP2 calculation, e.g. it overestimates the electrostatic interaction but underestimates the contribution of dispersion.

Harmonic vibrational frequencies of PPA, H_2O, and PPA$-(H_2O)$ were calculated at the MP2/aug-cc-pVDZ level. The output data are listed in Table 9. Available experimental frequencies are also listed for comparison. The intermolecular modes, denoted as "χ" in Table 9, correspond to the rocking or the stretching motions between the two monomers. It is the accuracy of these low vibrational frequencies that determines the accuracy of the vibrational partition function of PPA$-(H_2O)$. As empirically found in the case of formic acid$-(H_2O)$,[34] a very similar hydrate to PPA$-(H_2O)$, the intermolecular vibrations from MP2/aug-cc-pVDZ are randomly distributed around the experimental values with errors of $\pm 5\%$. Scaling, though a useful tool to remove the systematic error of the vibrational frequencies, may not of much help in the current case. In light of this, all the six intermolecular vibrational frequencies from MP2/aug-cc-pVDZ were used without scaling.

Besides the intermolecular vibrational frequencies, we also need to know the shifts of the intramolecular vibrational frequencies in the complex relative to the monomers in order to calculate the ZPE correction to the binding energy. Half of the sum of these shifts was predicted to be very small (15 cm^{-1}) by ab initio calculation and thus contribute little to the overall ZPE correction (802 cm^{-1}) to D_0.

The calculated value of K_p for PPA$-(H_2O)$ at different temperatures and a pressure of 1 bar are listed in Table 10. The fraction of PPA$-(H_2O)$ against the PPA monomer in the atmosphere, denoted as ξ, can be derived as

$$\xi = K_{p,PPA-(H_2O)}(p_{H_2O}/p^{\ominus}) \quad (4)$$

in which p_{H_2O} is the partial pressure of water vapor in bar. Under the typical atmospheric conditions as reported by Ellingson et al.,[35] the partial pressure of H_2O at the height of 2 km in midlatitude in summer was 0.0077 bar, corresponding to a relative humidity of 57%. From eq 4, the ratio of PPA$-(H_2O)$ to PPA was calculated as 1.4% under such atmospheric conditions. In the event of cloud formation when the relative humidity may be as high as 500%, the ratio of PPA$-(H_2O)$ to PPA can be expected to be 8−9 times larger.

With the partition functions, it is also possible to calculate the change of enthalpy $\Delta H^{\ominus}$ and entropy $\Delta S^{\ominus}$ for the formation of PPA$-(H_2O)$ at different temperatures.[36] The results are also shown in Table 10. In the range of 200−320 K, $\Delta H^{\ominus}$ changes by about 0.5 kJ mol^{-1} and $\Delta S^{\ominus}$ changes by about 1.9 J mol^{-1} K^{-1}, which only correspond to about 1.5% variation around their mean values. This suggests that both values can be considered stable in this small temperature range.

TABLE 10: Calculated Values of Change of Entropy and Enthalpy for the Formation of PPA$-(H_2O)$ and Its Equilibrium Constant (K_p) at Different Temperatures and Standard Pressure $p^{\ominus} = 1$ bar

T/K	$\Delta H^{\ominus}$/kJ mol^{-1}	$\Delta S^{\ominus}$/J mol^{-1} K^{-1}	K_p
200	−35.8	−120.8	1125.
210	−35.8	−120.8	403.0
220	−35.8	−120.7	158.5
230	−35.8	−120.6	67.65
240	−35.8	−120.4	31.01
250	−35.7	−120.3	15.14
260	−35.7	−120.1	7.820
270	−35.6	−120.0	4.244
280	−35.6	−119.8	2.408
290	−35.5	−119.6	1.421
300	−35.5	−119.4	0.8700
310	−35.4	−119.2	0.5500
320	−35.3	−119.0	0.3581

As a final remark, it should be noted that there are many factors that must have definitely introduced errors in the calculation of K_p. Among them, the errors in binding energy and the ZPE correction dominate as they appear in the exponent in eq 2. For example, a $\pm 10\%$ change of the ZPE correction would propagate an error of $\pm 40\%$ in K_p. This reminds us that even a factor of 2 error for K_p should not be surprising at all at the current level of calculation.

Acknowledgment. The support of EPSRC is gratefully acknowledged. We thank Eleanor Bains and Katie Daniels for their comments on the manuscript. B.O. expresses his thanks to the Chinese Ministry of Education and University of Oxford for jointly providing the China/UK scholarship for excellency to support his study in UK.

Supporting Information Available: (A) Cartesian coordinates. (B) Fitting of PPA monomer using Watson-A representation. (C) Calculation of orientation angle. This material is available free of charge via the Internet at http://pubs.acs.org.

References and Notes

(1) Nolte, C. G.; Fraser, M. P.; Cass, G. R. *Environ. Sci. Technol.* **1999**, *33*, 540.
(2) Saxena, P.; Hildemann, L. M. *J. Atmos. Chem.* **1996**, *24*, 57.
(3) Novakov, T.; Penner, J. E. *Nature* **1993**, *365*, 823.
(4) Facchini, M. C.; Mircea, M.; Fuzzi, S.; Charlson, R. J. *Nature* **1999**, *401*, 257.
(5) Canagaratna, M.; Phillips, J. A.; Ott, M. E.; Leopold, K. R. *J. Phys. Chem. A* **1998**, *102*, 1489.
(6) Fiacco, D. L.; Hunt, S. W.; Leopold, K. R. *J. Am. Chem. Soc.* **2002**, *124*, 4504.
(7) Priem, D.; Ha, T.-K.; Bauder, A. *J. Chem. Phys.* **2000**, *113*, 169.
(8) Kisiel, Z.; Białkowska-Jaworska, E.; Pszczółkowski, L.; Milet, A.; Struniewicz, C.; Moszynski, R.; Sadlej, J. *J. Chem. Phys.* **2000**, *112*, 5767.
(9) Kisiel, Z.; Pietrewicz, B. A.; Desyatnyk, O.; Pszczółkowski, L.; Struniewicz, I.; Sadlej, J. *J. Chem. Phys.* **2003**, *119*, 5907.
(10) Ouyang, B.; Starkey, T. G.; Howard, B. J. *J. Phys. Chem. A* **2007**, *111*, 6165.
(11) Coudert, L. H.; Hougen, J. T. *J. Mol. Spectrosc.* **1990**, *139*, 259.
(12) Stiefvater, O. L. *J. Chem. Phys.* **1975**, *62*, 233.
(13) Møller, C.; Plesset, M. S. *Phys. Rev.* **1934**, *46*, 618.
(14) Boys, S. F.; Bernardi, F. *Mol. Phys.* **1993**, *19*, 553.
(15) Frisch, M. J.; Trucks, G. W.; Schlegel, H. B.; et al. *GAUSSIAN 03*, revision C.02; Gaussian, Inc.: Wallingford CT, 2004.
(16) Pickett, H. M. *J. Mol. Spectrosc.* **1991**, *148*, 371.
(17) Bunker, P. R.; Jensen, P. *Molecular Symmetry and Spectroscopy*; NRC Research Press: Ottawa, 1998.

(18) Hartwig, H.; Dreizler, H. *Z. Naturforsch.* **1996**, *51a*, 923.
(19) Lawrence, C. K.; Saegebarth, E. *J. Chem. Phys.* **1971**, *54*, 4553.
(20) Dyke, T. R.; Muenter, J. S. *J. Chem. Phys.* **1974**, *60*, 2929.
(21) Atkins, P. W. *Physical Chemistry*; Oxford University Press: Oxford, 1994; Chap. 20.
(22) Dunning, T. H., Jr. *J. Chem. Phys.* **1989**, *90*, 1007.
(23) Woon, D. E.; Dunning, T. H., Jr. *J. Chem. Phys.* **1994**, *100*, 2975.
(24) Kendall, R. A.; Dunning, T. H., Jr.; Harrison, R. J. *J. Chem. Phys.* **1992**, *96*, 6796.
(25) Starkey, T. G. D. Investigation of Open-Shell Interactions, Phil. Thesis, University of Oxford, 2007.
(26) Nielsen, I. M. B.; Seidl, E. T.; Janssen, C. L. *J. Chem. Phys.* **1999**, *110*, 9435.
(27) Klopper, W. *Mol. Phys.* **2001**, *99*, 481.
(28) Hwang, R.; Huh, S. B.; Lee, J. S. *Mol. Phys.* **2003**, *101*, 1429.
(29) Tsuzuki, S.; Uchimaru, T.; Matsumura, K.; Mikami, M.; Tanabe, K. *J. Chem. Phys.* **1999**, *110*, 11906.
(30) Maçôas, E. M. S.; Khriachtchev, L.; Pettersson, M.; Fausto, R.; Räsänen, M. *J. Phys. Chem. A* **2005**, *109*, 3617.
(31) Sander, W.; Gantenberg, M. *Spectrochim. Acta, Part A* **2005**, *62*, 902.
(32) Herzberg, G. *Infrared and Raman Spectra of Polyatomic Molecules*; D. Van Nostrand Company, Inc: New York, 1945.
(33) Scott, A. P.; Radom, L. *J. Phys. Chem. A* **1996**, *100*, 16502.
(34) Ouyang, B.; Howard, B. J., to be submitted.
(35) Ellingson, R. G.; Ellis, J.; Fels, S. *J. Geophys. Res.* **1991**, *96*, 8929.
(36) Jensen, F. *Introduction to Computational Chemistry*; John Wiley & Sons Ltd: Chichester, 1999; Chap. 12.

JP802422B